Modeling the Giant Magellan Telescope dome seeing using fluid dynamics simulations

R. Conan[a], M. Van Dam[b], K. Vogiatzis[a], K. Das[a], and A. Bouchez[a]

[a]GMTO, 465 N. Halstead Avenue, Pasadana, CA
[b]Flat Wavefronts, P.O. Box 1060, Christchurch, New Zealand 8140

ABSTRACT

Seeing is a hindrance to telescope image quality. There are two components to the seeing: atmospheric seeing and dome seeing. The dome seeing, which stems from turbulence inside the dome, can be mitigated by proper venting of the telescope enclosure. The venting has two functions: it flushes the air trapped inside the dome and it thermalizes the telescope hence reducing turbulence by convection. For the Giant Magellan Telescope, the dome seeing has been modeled for 12 different configurations (wind speed and direction, enclosure vent and wind screen configurations) using computing fluid dynamics simulations. We simulate the correction of both atmospheric and dome seeing with a ground layer adaptive optics (GLAO) system based on an adaptive secondary mirror and three natural guide star Shack-Hartmann wavefront sensors. We present the results of the dome seeing simulations evaluating the telescope image quality with and without GLAO correction.

1. INTRODUCTION

The Giant Magellan Telescope (GMT) belongs to the next generation of giant segmented optical telescope alongside the Thirty Meter Telescope and the Extremely Large Telescope. The GMT follows a "Gregorian" two–mirrors aplanatic optical design with a parabolic primary mirror and an ellipsoid secondary mirror. Both primary and secondary are made of 7 circular segments.

In the following we introduce the model that is used to evaluate the dome seeing within the enclosure of the GMT. In Section 2, we describe the computational fluid dynamic (CFD) model that computes the fluctuations of the index of refraction inside the enclosure. The GMT dome seeing statistics is presented in Section 3. In Section 4, a Ground Layer Adaptive Optics (GLAO) simulation is used to mitigate the dome seeing effects.

2. COMPUTATIONAL FLUID DYNAMICS MODEL

The CFD model[2] uses a $12 \times 12 \times 5$ km^3 computational volume centered on the GMT observatory (Fig. 2) and the volume mesh is comprised of 28 millions cells with varying resolution. The observatory model includes the telescope, the telescope enclosure and the observatory summit support buildings (Fig. 1).

The CFD simulation computes and saves the time series of both pressure on structures at specified nodes and index of refraction in the enclosure volume. Time series are 400s long sampled at 20Hz. The wavefront aberrations due to the seeing in the enclosure are derived from ray tracing through the volume of index of refraction down to the telescope exit pupil.

A total of 12 different CFD cases were computed. Each case is a combination of a wind velocity and enclosure configuration (orientation, vents open/closed, wind screen stowed/deployed). The parameters of the 12 cases are given in Table 1. The enclosure orientation is given with respect to the predominant wind direction ((30º NNE)).

Computing the 12 cases in series would have taken approximately 60 days. CFD simulation generates a lots of data with each case producing ~ 0.5TB of data. To speed up the computing and manage the data, we use AWS cloud computing services. An Elastic Cluster was spawned from the cloud. The cluster size is automatically

Wind velocity [m/s]	Enclosure orientation [deg]	Vents	Wind screen
2	0	open	stowed
2	45	open	stowed
2	180	open	stowed
7	0	open	stowed
7	45	open	stowed
7	180	open	stowed
7	0	closed	deployed
7	45	closed	deployed
7	180	closed	deployed
12	0	closed	deployed
12	45	closed	deployed
12	180	closed	deployed

Table 1. CFD simulation cases

(a) CAD representation of the simplified enclosure components and surrounding buildings used in the study

(b) Telescope components including M1, M2, C-Ring, Truss etc. as used in present simulations
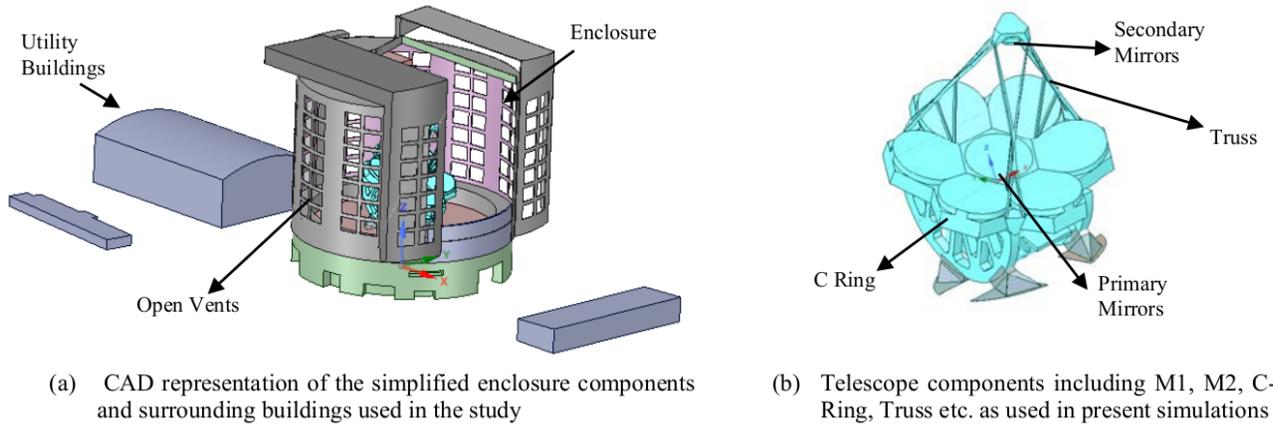
Figure 1. Observatory and telescope CAD models.

(a) Location of the Computational Domain within the Las Campanas Area

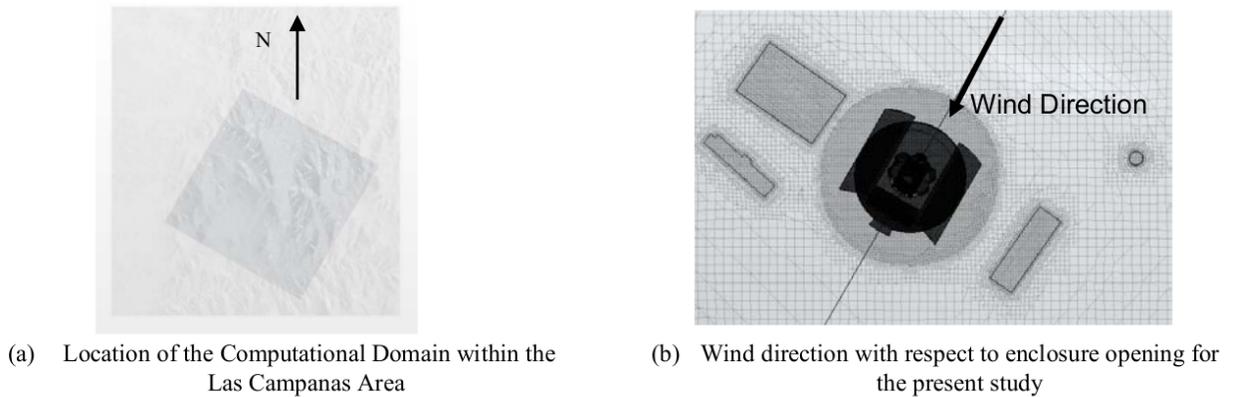(b) Wind direction with respect to enclosure opening for the present study

Figure 2. Computational domain and observatory orientation with respect to the predomimant wind direction.
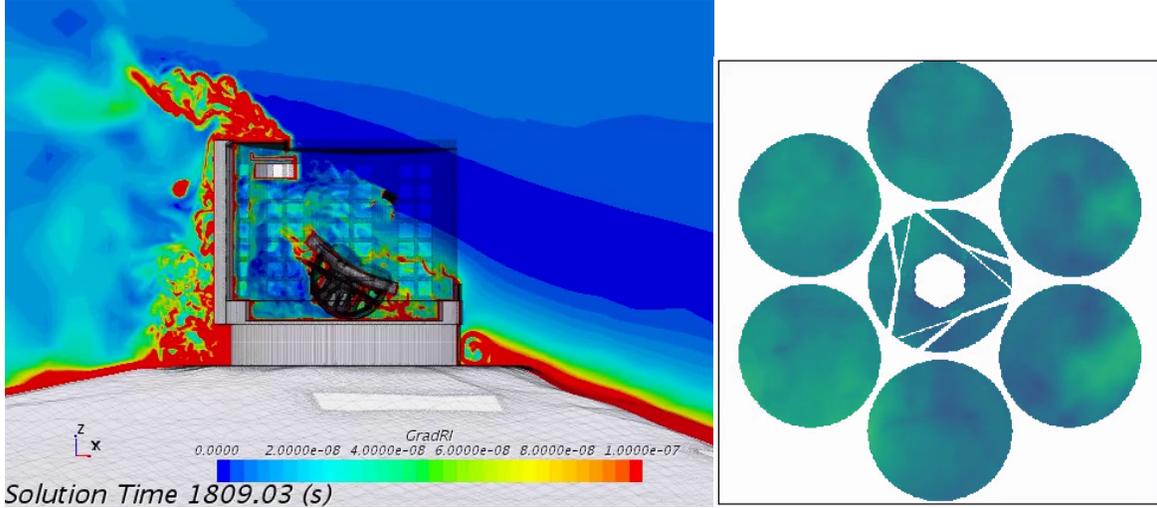
Figure 3. Index of refraction (left) and OPD (right) for an upwind case at 7m/s.
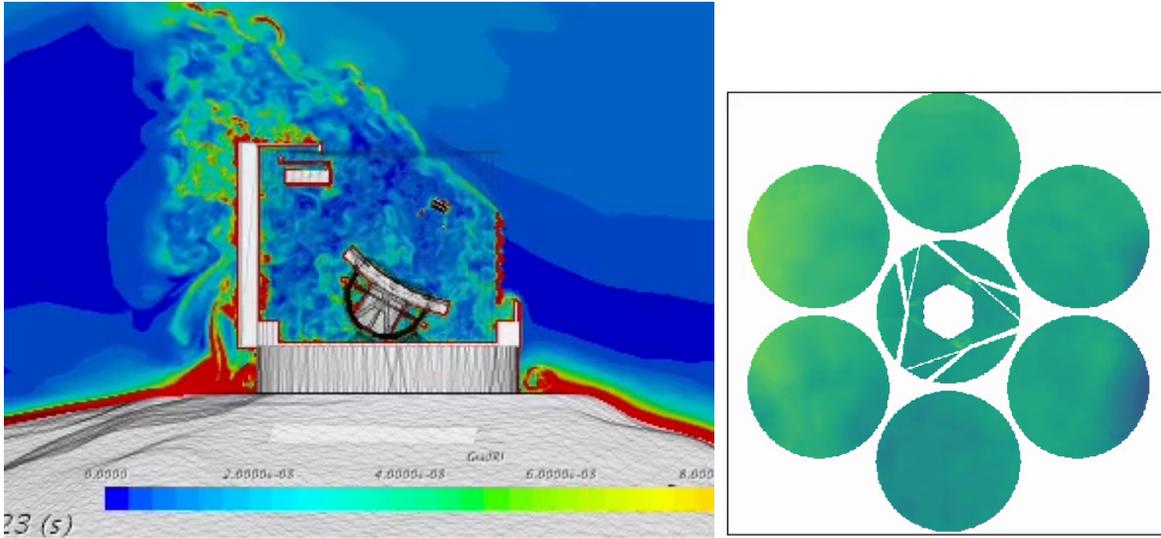

Figure 4. Index of refraction (left) and OPD (right) for an upwind case at 12m/s.

adjusted based on the number of required processes at any given time, hence avoiding the cost of idle hardware. The Elastic Cluster was setup with a maximum capacity of 2880 processes allowing to run 10 CFD cases in parallel and to complete the simulation in $\sim$ 1.5 weeks.

Examples of index of refraction in the enclosure and the corresponding OPDs are shown in Fig. 3, Fig. 4 and Fig. 5 for 7m/s, 12m/s and 2m/s, respectively.

3. DOME SEEING STATISTICS

In the following, we analyze the statistical properties of the wavefront aberrations in the telescope exit pupil induced by dome seeing.

Atmosphere seeing is know to be isotropic meaning that the wavefront error (WFE) RMS is the same at any point in the telescope pupil. Fig. 6 shows the WFE RMS maps of the dome seeing aberrations in the exit pupil . Dome seeing is clearly not isotropic.

Fig. 7 plots the temporal decorrelation of the dome seeing wavefront for the 12 simulation cases. It shows that the dome seeing wavefront typical decorrelation time scale τ_0 depends on the wind speed, the wind direction
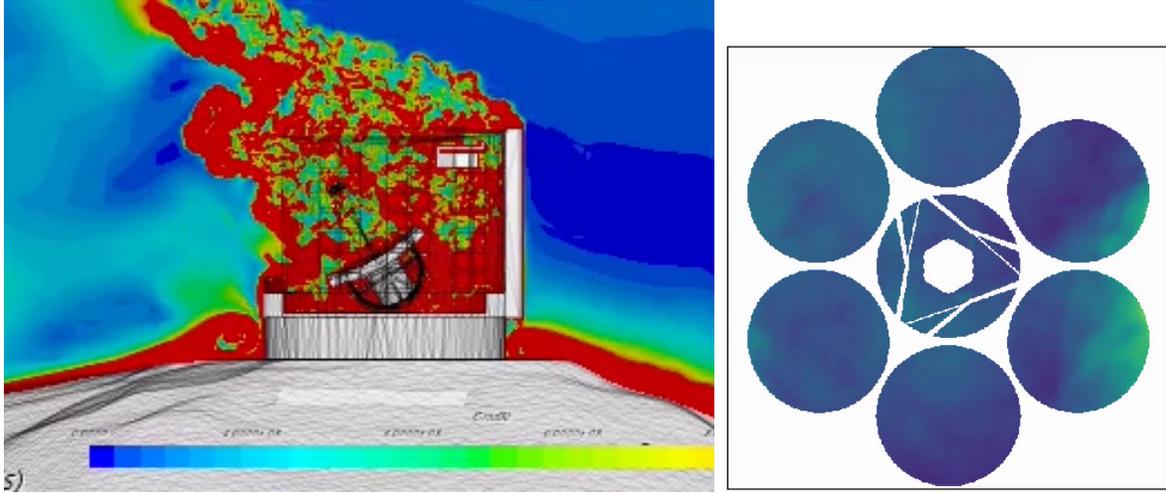
3

Figure 5. Index of refraction (left) and OPD (right) for an downwind case at 2m/s.
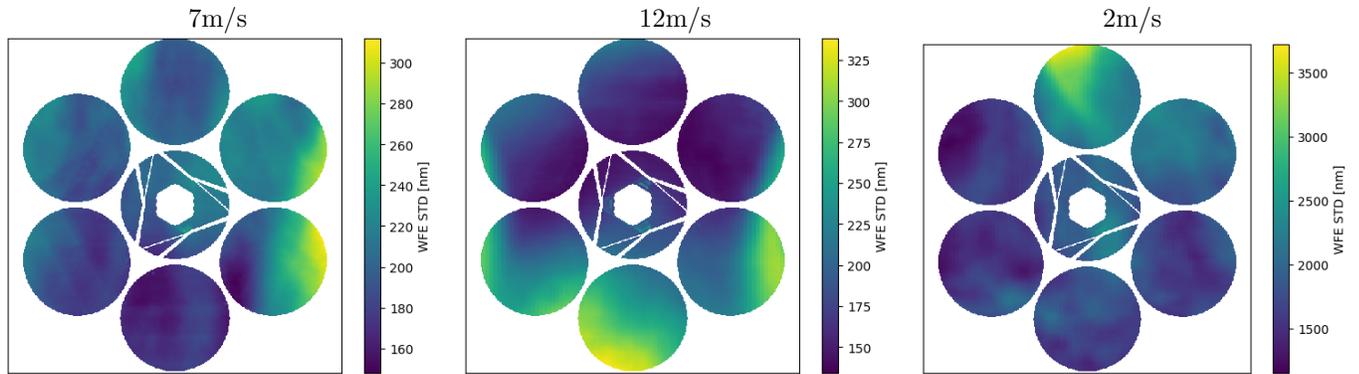

Figure 6. WFE RMS in the telescope exit pupil.

and the configuration of the enclosure.

Fig. 8 shows the total WFE RMS and the residual error (or fitting error) after correction of the wavefront with a 25×25 and a 51×51 actuators deformable mirror. Dome seeing wavefront error increases at low wind speed and when the telescope turns away from facing the wind.
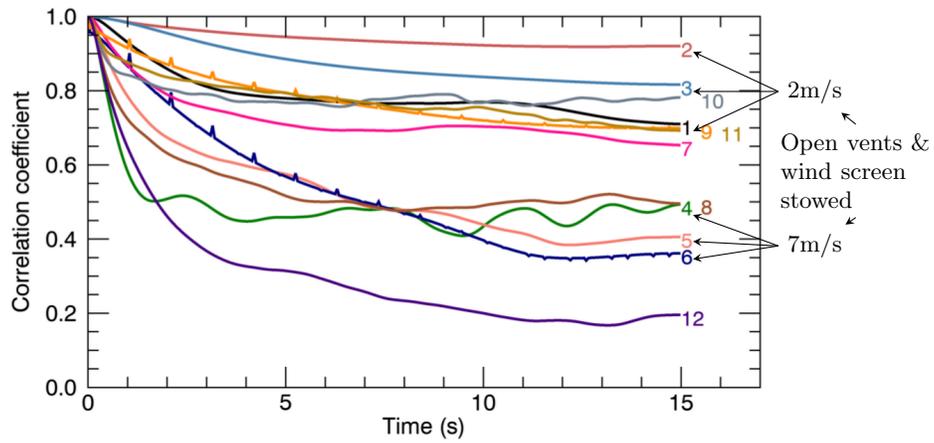
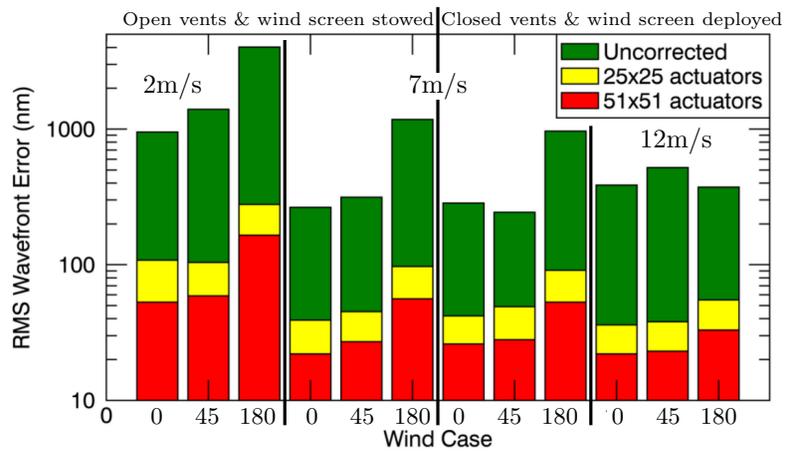Figure 7. Dome seeing wavefront temporal decorrelation.

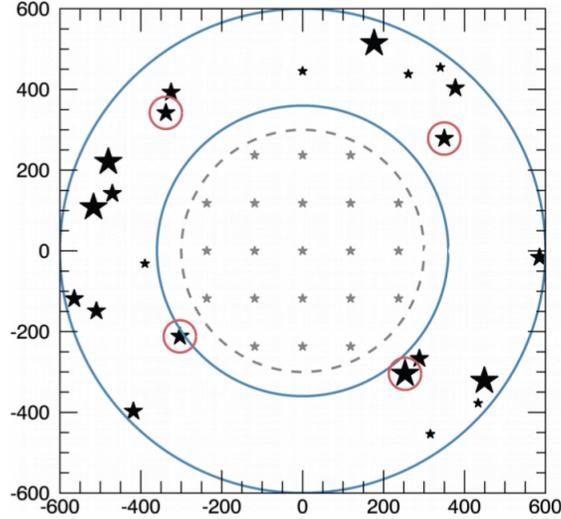Figure 8. Dome seeing wavefront total and fitting errors.

Figure 9. GLAO asterism, the red circles indicate the guide stars, the optimization field is show as the dashed gray circle.
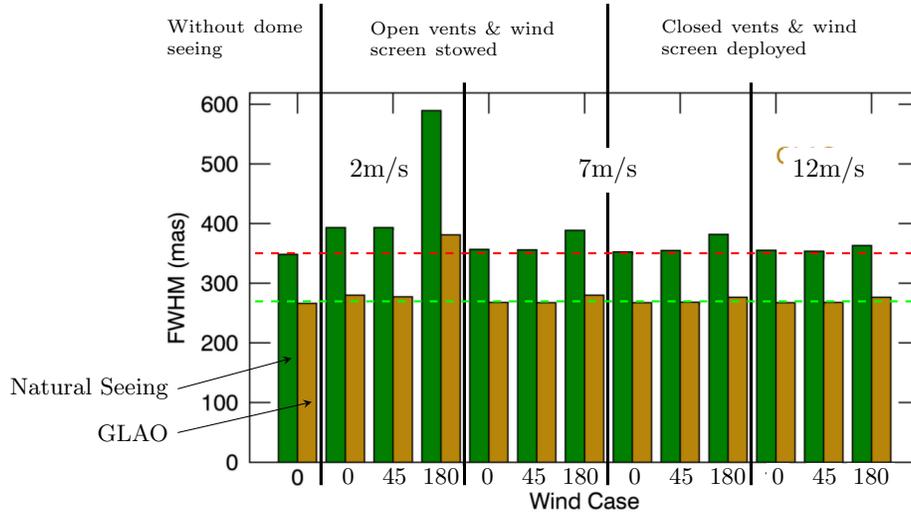

Figure 10. GLAO FWHM without GLAO (green) and with GLAO (yellow)

4. GROUND LAYER ADAPTIVE OPTICS

A GLAO[1] simulation was setup with 4 natural guide stars located between a radius of 6' and 10' arc–minute (Fig. 9). Wavefront sensing is performed with four 51×51 Shack–Hartmann wavefront sensor with a 88Hz frame rate. The simulation includes both atmosphere and dome seeing. The GLAO algorithm was setup to minimize the wavefront over a 10' diameter field–of–view.

Fig. 10 shows the FWHM of a point source in the focal plane with and without GLAO correction. The first 2 bars do not include the dome seeing. In the natural seeing mode (no GLAO), the dome seeing degrades the image mainly at low wind speed and when the enclosure is downwind. With GLAO, the dome seeing degradation is nearly fully corrected to the same level than when the dome seeing is not accounted for. The only notable exception is for the downwind 2m/s case where there is not enough flushing and the turbulence in the dome is stirred by convective effects induced by the telescope structure differential temperature with respect to the ambient air.

6

5. SUMMARY

- We have developped the mean to compute high spatial and temporal resolution dome seeing CFD simulation for a sweeping range of cases in a reasonable amount of time at an affordable cost

- Dome seeing is anisotropic and its decorrelation time is highly dependent upon the wind speed, the observatory orientation with respect to the wind direction and the enclosure configuration

- GLAO can mitigate the effects of dome seeing in most cases

- We plan to redo this exercise as the design evolved for both the enclosure and the telescope

REFERENCES

[1] R. Conan M. van Dam and A. Bouchez. Effect of Dome Seeing in Ground Layer Adaptive Optics. Technical Report FWN 105, GMTO, November 2018.

[2] Konstantinos Vogiatzis, Kaushik Das, George Angeli, Bruce Bigelow, and Will Burgett. Computational fluid dynamics modeling of GMT. In *SPIE*, volume 10705 of *Society of Photo-Optical Instrumentation Engineers (SPIE) Conference Series*, page 107050R, Jul 2018.